ADVANCED ENERGY MATERIALS
www.advenergymat.de

On-Fabrication Solid-State N-Doping of Graphene by an Electron-Transporting Metal Oxide Layer for Efficient Inverted Organic Solar Cells

*Hobeom Kim, Jinwoo Byun, Sang-Hoon Bae, Towfiq Ahmed, Jian-Xin Zhu, Sung-Joo Kwon, Yeongjun Lee, Sung-Yong Min, Christoph Wolf, Hong-Kyu Seo, Jong-Hyun Ahn, and Tae-Woo Lee**

Graphene is a promising transparent conducting electrode for organic electronic devices[1] due to its excellent electrical, optical and mechanical properties.[2] Especially, graphene grown by chemical vapor deposition (CVD) method is suitable for use in electrodes of organic electronics due to its low sheet resistance R_s and ease of synthesis and patterning.[3]

Organic solar cells (OSCs) are light-weight, flexible, and have the potential to be produced over large areas at low cost; they have recently exceeded power conversion efficiencies (PCEs) of 10% for both single and tandem structure, and are therefore considered to be promising power-supply devices for future electronics.[4,5] OSCs with inverted structure (iOSCs) have been regarded as a better configuration than conventional structure because iOSCs do not need (i) acidic poly(3,4-ethylene dioxythiophene):poly(styrenesulfonate) (PEDOT:PSS) which can cause corrosion of ITO electrodes, or (ii) metallic cathode interlayers with low work function (e.g., Ca, Ba) which can be easily oxidized, but instead can use air-stable interfacial layers (e.g., ZnO, TiO_x, MoO_3).[6–10] For these reasons, iOSCs based on CVD-grown graphene electrodes should be developed. However, to develop an iOSC that uses graphene as an electrode, three challenges must be overcome.

(1) Deposition of a uniform electron transport layer (ETL) on graphene electrodes is a difficult task. For example, sol–gel derived ZnO, which is widely used as an ETL in iOSCs, cannot be easily coated on hydrophobic graphene surface because the precursor solution of ZnO is generally composed of hydrophilic alcohol-based solvents, so dewetted regions form. The nonuniform ZnO layer with a lot of large-size dewetted regions on graphene can cause short-circuit current and leakage current in the iOSCs because the dewetted regions cannot efficiently block holes and have protruding edges over 1 μm in height which is much higher than general thickness of photo-active layer of organic solar cells (Figure S1, Supporting Information).

(2) Conventional graphene n-doping methods are undesirable. Substitutional n-doping graphene significantly degrades its electrical conductivity because incorporation of dopant impurities destroys the inherent lattice structure of graphene.[11–14] Nondestructive surface doping,[15–17] is also not so effective in graphene cathodes of iOSCs, because charge carriers flow vertically through the device, so a layer of an insulating chemical surface dopant on graphene can impede efficient transfer of charges generated in a photo-active layer to electrodes in iOSCs.

(3) Although studies on the interface between graphene and an overlying interfacial layer have been reported in the literatures, much more intensive research on the interface physics and mechanism of charge transfer at the interface is required to clearly understand correlation with device efficiency of organic solar cells.[18–21]

In this study, solid-state n-doping of graphene directly by a nonvolatile charge transporting layer during device fabrication which would be an ideal approach was demonstrated. First-principles calculations using density functional theory (DFT) were performed to reveal solution-processed solid-state n-doping of graphene induced by electron transfer from ZnO. The n-doping effect was also experimentally confirmed by Raman spectroscopy analysis and Dirac point shift of graphene field-effect transistors (GFETs) after overcoming the problem of poor film formation of ZnO on graphene by adding a fluorosurfactant, Zonyl, to the precursor solution of ZnO. By exploiting the uniform ZnO film on graphene and the n-doped graphene, we successfully developed highly-efficient iOSCs with the graphene as a cathode without additional chemical doping, and achieved a high PCE = 7.5%, which was the same as that of an otherwise-identical device with an ITO cathode. To date, this is the highest reported PCE among single-junction OSCs with graphene

H. Kim, J. Byun, S.-J. Kwon, Y. Lee, Dr. S.-Y. Min, C. Wolf, H.-K. Seo, Prof. T.-W. Lee
Department of Materials Science and Engineering
Pohang University of Science and Technology (POSTECH)
Pohang, Gyungbuk 790-784, South Korea
E-mail: twlee@postech.ac.kr, taewlees@gmail.com
S.-H. Bae, Prof. J.-H. Ahn
School of Electrical and Electronic Engineering
Yonsei University
Seoul 120–749, South Korea
Dr. T. Ahmed
Theoretical Division
Los Alamos National Laboratory
Los Alamos, NM 87545, USA
Dr. J.-X. Zhu
Center for Integrated Nanotechnologies
Los Alamos National Laboratory
Los Alamos, NM 87545, USA

DOI: 10.1002/aenm.201600172

electrodes. To understand this result, we conducted systematic analysis of light harvesting and recombination kinetics. Also, we revealed electron transfer mechanism at the interface between graphene cathode and the electron transporting ZnO layer by analyzing photoemission spectroscopy (PES) results.

All calculations are performed using the plane-wave pseudo-potential code Vienna ab initio simulation package (VASP)[22–24] under the generalized gradient approximation of Perdew, Burke, and Ernzerhof (PBE).[25] For atomic core-levels, we have used projected augmented wave (PAW) potentials[26,27] treating the 2*s*2*p* of O, 4*s*3*d* of Zn, and 2*s*2*p* of C as the explicit valence electrons. A maximum energy cutoff of 400 eV is used for plane-wave basis set. The Bulk ZnO has hexagonal unit cell with P63MC space group (lattice constants: a = 3.2494 Å, c = 5.2054 Å, $\alpha = \beta = 90°$, $\gamma = 120°$). For the combined ZnO/graphene system, we have taken a supercell with $4 \times 4 \times 6$ unit cells of ZnO and $5 \times 5 \times 1$ unit cells of graphene, and thus making both ZnO slab and 2D graphene sheet commensurate with each other. The lattice constants of this hexagonal supercell are $a = b = 12.997$ Å, $c = 80$ Å, $\alpha = \beta = 90°$, and $\gamma = 120°$. There are in total 96 Zn, 96 O, and 50 C atoms in this supercell.

We benchmarked the density of states (DOS) of isolated ZnO slab and 2D graphene sheet and have relaxed our ZnO/graphene heterostructure using van der Waals (vdW) interaction. To keep the calculation expense reasonable, we have only considered six layers of ZnO planes in 001 direction. To mimic the bulkness of ZnO layer, we kept the ZnO ions frozen but relaxed the C ions in graphene using vdW interaction.

To incorporate the vdW interaction between the graphene and ZnO surface, we have used optB86b-vdW functional where the exchange functionals were optimized for the correlation part.[28] Therefore, the local density approximation (LDA) correlation part present in the PBE functional is removed by using the parameter AGGAC = 0.000 in the input file in order to avoid double-counting.

For ionic relaxation of ZnO/graphene systems, we have used the Γ point to sample the Brillouin zone, while we used $5 \times 5 \times 1$ k-points in the Brillouin zone for all other calculations.

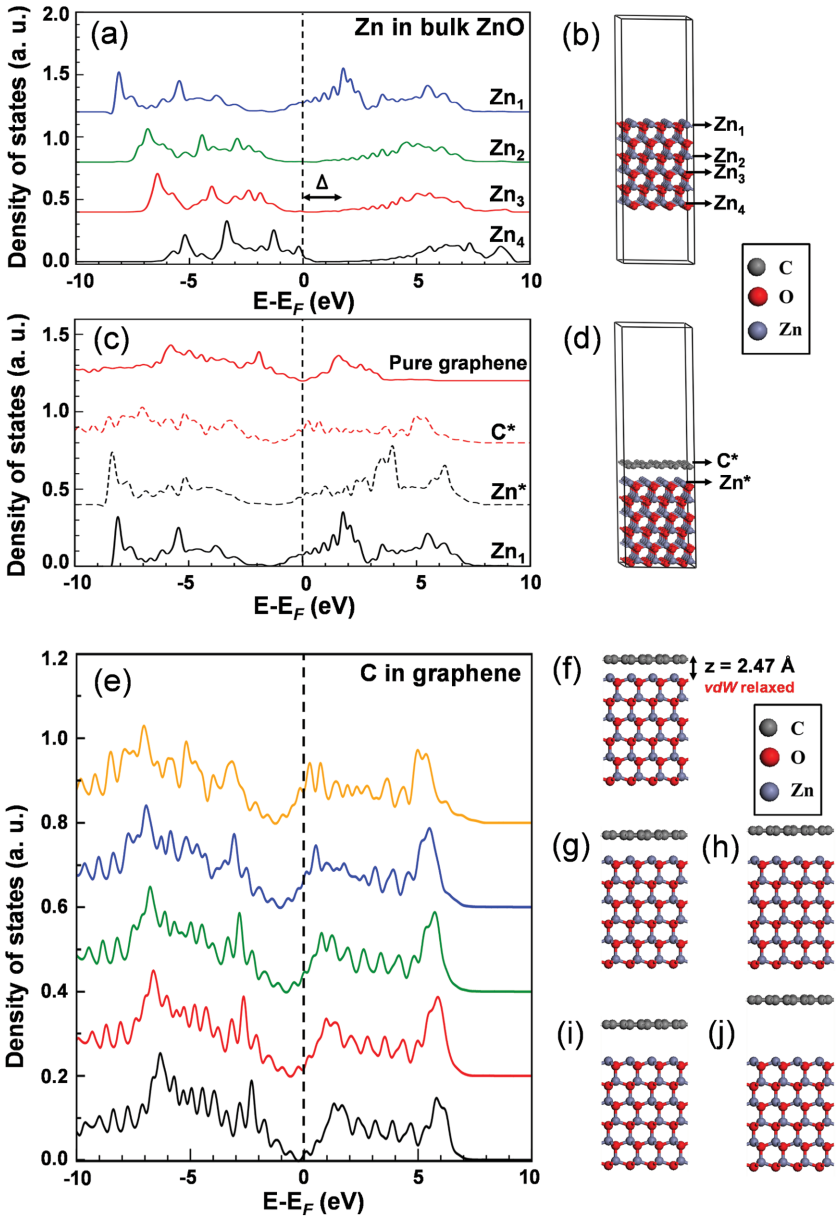

Figure 1. Curves in (a) are DOS of representative Zn ions Zn_1 (oxygen poor ZnO 001 surface), Zn_2 (bulk like), Zn_3 (bulk like), and Zn_4 (oxygen rich ZnO 001 surface). These particular Zn ions are identified in (b). Δ shows the band gap in Zn_3 ions which is comparable to the band gap in bulk ZnO. Curves in (c) show electron transfer trend from surface Zn* ions to C* ions of graphene for the combined ZnO/graphene system as identified in (d). DOS of Zn_1 ions in pure ZnO slab is shown by the lowest curve (solid black) while DOS of pristine graphene is shown by the top most curve (solid red) as reference points to compare electron transfer in the combined system. e) Distance dependence of DOS of C atoms in graphene for the combined ZnO/graphene system. The curves in the left panel show the DOS of C atoms in graphene corresponding to the configuration displayed by (f) (orange), (g) (blue), (h) (green), (i) (red), and (j) (black) on the right. The top most curve (orange) is DOS of C atoms when graphene position is relaxed with vdW interaction in our DFT calculation. The other configurations (f)–(j) are for increasing distances between graphene and ZnO surface. The vertical dashed lines in (a), (c), and (e) are at the Fermi energy.

To keep the calculation affordable, we have taken a slab of ZnO with six Zn and O planes (**Figure 1**b). In Figure 1a, DOS of Zn sites at different layers are presented. We note that the DOS of Zn_2 and Zn_3, which are located near the central part of the slab, show bulk ZnO like behavior with band gap of 2.2 eV. For this we have used DFT with PBE exchange correlation functional. Experimental band gap in bulk ZnO is 3.44 eV,[29] which is underestimated due to the well-known limitation of ground state nature of DFT, and can be treated using

quasiparticle correction (e.g., GW[29,30]). But for the purpose of the current discussion, such treatments are not essential as long as our DFT calculations correctly determine the presence of semiconducting band gap. This also confirms the validity of our calculations in determining the semiconducting or metallic nature of a given system. Interestingly, we note that due to surface termination in the ZnO slab, the preservation of stoichiometry makes one of the surfaces oxygen poor and the other one oxygen rich. Such asymmetric oxygen distribution makes the Zn ions on top surface (e.g., Zn_1) electron doped. However, the Zn ions in the central region (e.g., Zn_2, Zn_3) show band gap in the DOS (Figure 1a) mimicking the Zn ions in bulk ZnO. When combined into a hetero-structure ZnO/graphene system, our DFT calculation finds electron transfer from surface of ZnO to graphene. Figure 1c shows the DOS of C atoms in graphene in the combined system. Comparing with pristine graphene (top solid red curve in Figure 1c), the C atoms in combined ZnO/graphene are clearly electron doped. On the other hand, Zn in the combined system (Zn*) is found to loose electrons (dotted black in Figure 1c) when compared with the DOS of Zn_1 ion in the pure ZnO slab. We also investigated how the graphene becomes increasingly electron doped as it approaches ZnO surface (Figure 1e). The optimized distance between graphene and ZnO is 2.47 Å and the Dirac point in graphene is on the left of Fermi energy for this distance, which clearly indicates the electrons doping or transfer onto graphene from ZnO.

To realize the solid-state n-doping of graphene experimentally, a uniform ZnO layer on graphene surface should be formed. However, the pristine ZnO did not fully cover the hydrophobic graphene surface, because the precursor solution of ZnO is composed of hydrophilic mixed alcohol solvents (2-methoxyethanol (2-ME) and methanol with 1:1 volume ratio). To overcome this problem, we added small amount of Zonyl (0.8 vol%) to the precursor and it resulted in formation of a homogeneous ZnO layer on graphene surface (**Figure 2**; Figure S1, Supporting Information). The high quality of the Zonyl-added ZnO (ZZO) film on the graphene surface can be attributed to the amphiphilic chemical structure of Zonyl which consists of ethylene glycol and fluorinated groups in a molecule.[31] To be specific, ethylene glycol groups help itself be well dissolved in the precursor solution and fluorinated groups dominantly lower surface tension of the solution.[32]

One signal of doped graphene can be observed from the change in the intensity ratio 2D/G of Raman spectroscopy after doping. The 2D/G ratio with ZZO layer on graphene was 20% lower than that with pristine graphene (Figure 2d) Also, upshift of G bands from 1584 to 1593 cm^{-1} was observed; this result indicates that graphene is n-doped by ZZO and is in agreement with previous works in which the n-doping of CVD-grown graphene was explained.[33–35] It is well known that G peak shift and change in I_{2D}/I_G ratio occur as graphene is doped because the Fermi surface of graphene changes by the doping condition. Specifically, since the doping of graphene makes the Kohn anomaly moves away from $\mathbf{q} = \mathbf{0}$ point in the energy-momentum graph, we can observe the G peak shift and change in I_{2D}/I_G ratio.[36,37]

To further confirm the n-doping of graphene, we fabricated GFETs with bottom-gate, top-contact structure. The GFETs consisted of a 300-nm-thick SiO_2 dielectric layer on Si substrate, and patterned Ti/Au as source and drain electrodes deposited using thermal evaporation. The channels in the devices had length = 100 µm and width = 1500 µm, and were composed of either single-layer graphene or ZZO coated single-layer graphene. After measuring electrical characteristics of the devices, we compared the Dirac point positions of each device to demonstrate the n-doping effect of ZZO on graphene. The pristine graphene transistor showed a p-type behavior with a positive Dirac point >50 V, which is caused unintentionally by moisture, oxygen, or defects during the general wet-transfer process of CVD-grown graphene;[16,38] the device with ZZO layer showed strong n-type behavior with a Dirac point near –60 V (Figure 2e). This result indicates that graphene was strongly n-doped by ZZO and that electron transfer from ZZO layer to graphene occurred which is in agreement with our results of DFT calculation.

The n-doping of graphene is directly correlated to energy level change in the system. To examine this, we analyzed ultraviolet photoemission spectroscopy (UPS) spectra of graphene and ZZO deposited graphene as a function of thickness of ZZO. The cutoff energy of UPS spectrum showed a clear shift to higher binding energy as increasing thickness of ZZO until 17.6 nm which means that vacuum level shift occurs with deposition of ZZO on graphene (Figure 2f). Also, onset point shift was observed with the same trend as cutoff energy shifted (Figure 2g).

Based on the UPS spectra and band gap of ZZO which is obtained from its absorption spectrum (Figure S3d, Supporting Information), the schematic energy band diagram of graphene, ZZO and interface between them is presented (Figure 2h). Despite the existence of Schottky barrier and another barrier arising from band bending at each side of graphene and ZZO, charge transfer through the interface where pinned contact is formed can be facilitated from both directions according to Bardeen model. Bardeen described that if the density of surface states is sufficiently high and contact is made with a metal, barrier height and band bending become independent of metal work function and thereby pinned contact where charges can tunnel easily across the interface.[39] Since ZZO layer is formed by solution process in ambient condition, it has defects such as intrinsic oxygen vacancies and impurities which are responsible for the presence of surface states with high density.[40,41] Therefore, we can expect that graphene can effectively collect charges from ZZO and the iOSCs with the graphene cathode can operate efficiently.

Also, we analyzed X-ray photoemission spectroscopy (XPS) C1s spectra where shift of C—C peak of graphene was observed after deposition of ZZO from 284.4 to 285.9 eV (Figure S4, Supporting Information). The large shift evidently indicates n-doping of graphene by ZZO layer.

Based on the n-doping effect and formation of a uniform film of ZZO on graphene, we developed graphene-based iOSCs where ZZO plays a double role as an n-type dopant for graphene and an ETL. The device consists of a bottom three-layer stacked CVD-grown graphene cathode layer, a 100 nm-thick layer of ZZO, and a 120-nm-thick photo-active layer consisting of a bulk-heterojunction (BHJ) of thieno[3,4-b]-thiophene/benzodithiophene (PTB7) and [2]-phenyl-C_{71}-butyric acid methyl

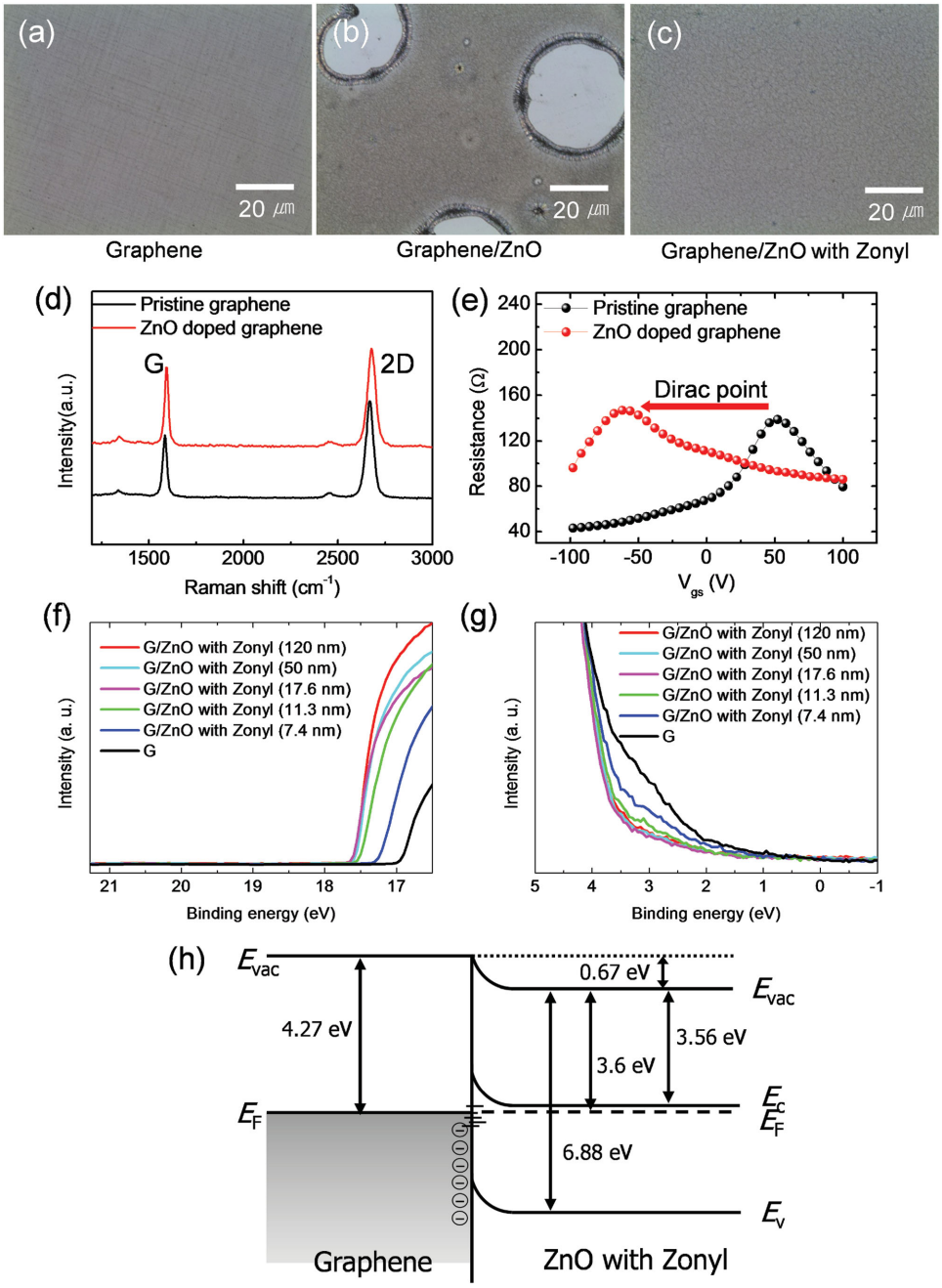

Figure 2. Optical microscopy images of (a) graphene, (b) graphene/ZnO, and c) graphene/ZnO with Zonyl (ZZO). d) Raman spectra of the pristine graphene (black) and ZZO doped graphene (red). e) Resistance of the pristine graphene transistor (black) and ZZO doped graphene transistor (red) as a function of applied bottom gate voltages (V_{ds} = 0.1 V). f) Cutoff and (g) onset region of UPS spectra of graphene and ZZO on graphene as increasing thickness of ZZO. h) Energy-band diagram of graphene/ZZO.

ester ($PC_{71}BM$) (**Figure 3**b). The device was completed by thermal evaporation of a 5 nm-thick MoO_3 hole interfacial layer and a 100 nm-thick Ag layers as an anode (Figure 3a). The energy level diagram (Figure 3c) shows good matching of each level for charge transfer and collection. For comparison, we fabricated otherwise-identical devices that used ITO as a cathode.

Current density–voltage (J–V) characteristics of iOSCs with graphene or ITO cathodes with varying the ETL were measured under simulated AM 1.5 with 100 mW cm^{-2} illumination (**Figure 4**a). The iOSC device based on the graphene cathode with a ZZO layer achieved open-circuit voltage (V_{OC}) = 0.766 V, short-circuit current (J_{SC}) = 15.87 mA cm^{-2}, fill factor (FF) = 61.8%, and PCE = 7.51%; these were quite similar to those of the device with ITO cathode and ZZO layer, which had V_{OC} = 0.759 V, J_{SC} = 14.91 mA cm^{-2}, FF = 66.4% and PCE = 7.51% (**Table 1**). The graphene device had a slightly higher J_{SC} but slightly lower FF than did the ITO device, so the

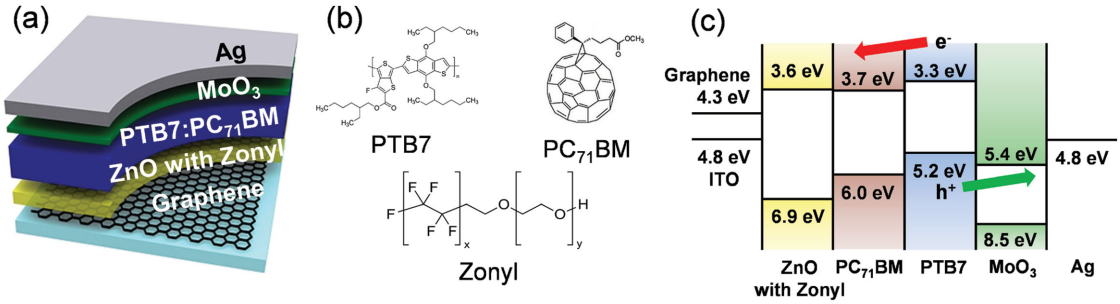

Figure 3. a) Schematic device configuration of iOSC device based on CVD-grown graphene cathode. b) The chemical structures of photo-active materials (PTB7 and $PC_{71}BM$) and fluorosurfactant Zonyl which was used for modification of precursor solution. c) Energy level of materials used for devices.

devices had the same PCE. The graphene device had higher external quantum efficiency (EQE) (Figure 4b) and higher transmittance of the cathode layer (Figure 4c) than did the ITO device, particularly in the blue and orange-red regions. Moreover, higher optical electric field is situated in the photo-active layer of the graphene device according to calculation using the transfer matrix method (Figure S6, Supporting Information). Based on the higher average transmittance of graphene and the higher optical electric field in the PTB7:$PC_{71}BM$ layer of the graphene device, absorbance of PTB7:$PC_{71}BM$ on graphene was also higher than that on ITO (Figure 4d); this difference is the reason for J_{SC} being higher in the graphene device than in the ITO device.

To investigate why J_{SC} was higher in the graphene device than in the ITO device, we plotted net photocurrent density $J_{ph} = J_L - J_D$, where J_L and J_D are respectively the photocurrent density under illumination and in the dark, as a function of effective voltage $V_{eff} = V_O - V_A$, where V_O is the compensation voltage at which $J_{ph} = 0$ and V_A is the applied bias voltage (**Figure 5**a); this is a powerful method to analyze light harvesting and the underlying physics of photovoltaic devices.[42,43] Here, we assumed that all photogenerated excitons dissociate into free charge carriers at a high V_{eff} (here, $V_{eff} = 1.8$ V). Thus, the amount of absorbed incident photon flux is the only factor that limits the saturation current density J_{sat}. Then we calculated the maximum exciton generation rates G_{max} from the equation given as $J_{sat} = eG_{max}L$, where e is the charge on an electron and L is the thickness of the photo-active layer, 120 nm in our system. The graphene device had $G_{max} = 8.65 \times 10^{27}$ m^{-3} s^{-1} and the ITO device had $G_{max} = 8.22 \times 10^{27}$ m^{-3} s^{-1}. The higher G_{max} of graphene device implies higher light absorption which can be attributed to higher transmittance of graphene and higher optical electric field of the graphene device, which results in higher J_{SC} and EQE, all compared to the ITO device.

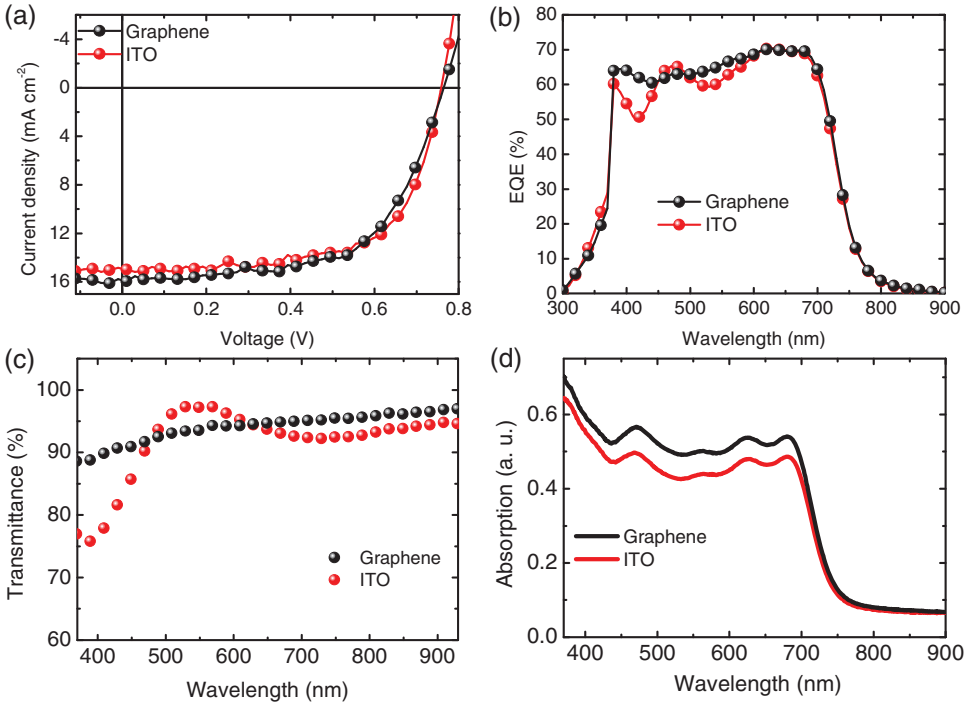

Figure 4. a) Current density versus voltage (J–V) characteristics and (b) EQE characteristics of iOSC devices. c) Transmittance of graphene and ITO cathode. d) Absorption spectra of PTB7:$PC_{71}BM$ on graphene/ZZO and ITO/ZZO.

Table 1. Summary of photovoltaic parameters of devices in Figure 4a.

Cathode	V_{oc} [V]	J_{sc} [mA cm^{-2}]	FF [%]	PCE [%]	
				Average	Best
Graphene	0.766	15.87	61.8	7.30 ± 0.15	7.51
ITO	0.759	14.91	66.4	7.44 ± 0.08	7.51

To gain insight of the recombination kinetics of our devices, we measured J–V characteristics as a function of the light intensity (Figure S1, Supporting Information) and plotted V_{OC} (Figure 5b) and J_{SC} (Figure 5c).[44,45] At the open-circuit condition where the photocurrent is zero, recombination of all photogenerated charges occurs and reveals information about the recombination mechanism in a device. V_{OC} of BHJ OSCs can be expressed as

$$V_{oc} = \frac{1}{e}\left(E_{LUMO}^{Fullerene} - E_{HOMO}^{Polymer} - \Delta\right) - \frac{kT}{e}\ln\left(\frac{n_e n_h}{N_c^2}\right) \quad (1)$$

where n_e and n_h are electron and hole densities, respectively, at open-circuit condition in the BHJ, and are proportional to the light intensity; N_c is the effective density of states; $E_{LUMO}^{Fullerene}$ is the lowest unoccupied molecular orbital (LUMO) energy level of fullerene; $E_{HOMO}^{Polymer}$ is the highest occupied molecular orbital (HOMO) energy level of donor material; Δ represents energy shift by band tailing of LUMO of acceptor and HOMO of donor, which originates from disorder of solution cast and phase separated polymer and fullerene regions; e is the charge on an electron; k is the Boltzman constant; and T is absolute temperature. If nongeminate recombination is the dominant mechanism, then $n_e n_h = G/\gamma$, where G is the generation rate of the bound electron–hole pair and γ is the Langevin recombination constant. Because G is proportional to the incident light intensity I, Equation (1) can be rewritten as

$$\delta V_{oc} = \left(\frac{kT}{e}\right)\ln(I) + \text{const.} \quad (2)$$

where kT/e is the slope of V_{OC} versus $\ln(I)$. Otherwise, if geminate recombination is the dominant mechanism, both n_e and n_h are proportional to the light intensity and the slope becomes 2 kT/e.[44] The slope was 0.99 kT/e in graphene devices and 1.00 kT/e in ITO devices; these results indicate that nongeminate recombination is the main loss mechanism in them and that geminate recombination is negligible. This result is in agreement with a previous report that devices with PTB7:$PC_{71}BM$ processed from chlorobenzene (CB) with additive, 1,8-diiodooctane (DIO) which is the same photo-active layer as in our system, are dominated by nongeminate recombination but by geminate recombination without DIO.[46]

We also measured J_{SC} of the devices as a function of I (Figure 5c) to further understand the recombination mechanism in them. J_{SC} follows a power-law dependence on I as $J_{SC} \propto I^{\alpha}$ where $\alpha = 0.96$ in graphene device and $\alpha = 1.00$ for ITO device. $\alpha \approx 1$ indicates that all the dissociated photoexcited charges were swept out before nongeminate recombination occurs.[47,48] The larger deviation of α from linear scaling for graphene device means that nongeminate recombination has more influence on graphene device than on ITO device. Considering the result of these analyses of recombination kinetics, and the fact that the device configuration of both devices is the same except for the cathode, we conclude that a little more nongeminate recombination in the graphene device than in the ITO device occurs due to a little less efficient collection to the graphene cathode arising from a high R_s, traps in the PMMA residues, and thus a little more build-up of space charges.[49] Therefore, the graphene devices showed a little less FF compared with the ITO devices.

In summary, we theoretically observed electron transfer from ZnO to graphene which in turn leads n-doping of graphene

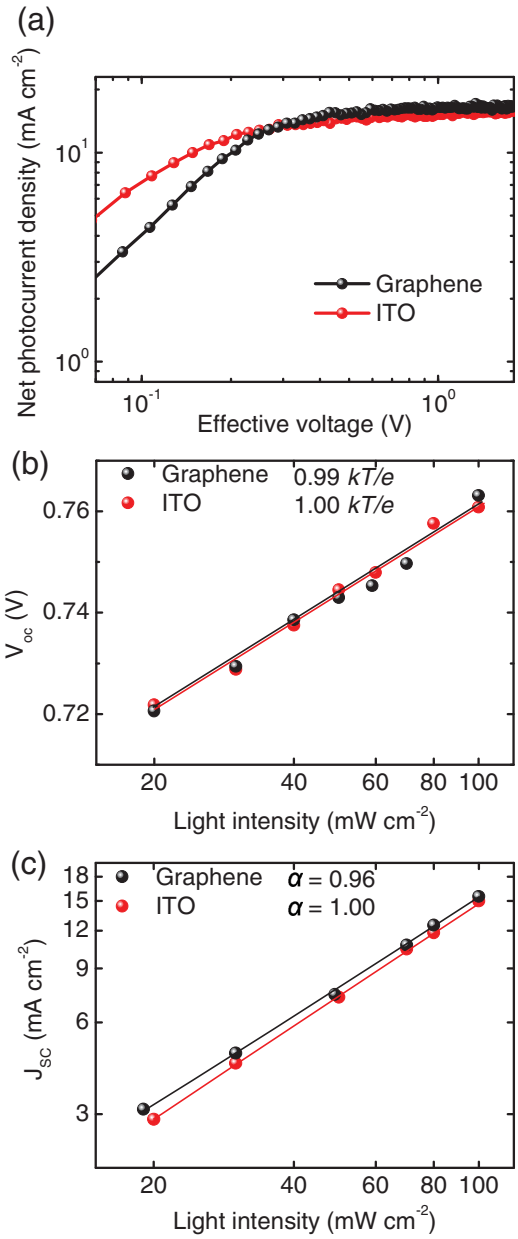

Figure 5. a) Net photocurrent density versus effective voltage (J_{ph}–V_{eff}) of iOSC devices with graphene and ITO cathode. Variation of (b) V_{OC} and (b) J_{SC} as a function of light intensity for devices with ITO and graphene cathode.

from first-principles DFT calculations. After obtaining a uniform film of ZnO on graphene by adding fluorosurfactant, Zonyl, into ZnO precursor solution, we experimentally confirmed the effective solid-state n-doping of graphene by analysis of Raman spectroscopy and GFETs. Also, study on the graphene interface physics by UPS and XPS presented efficient electron transfer can occur from the ZZO to graphene. This indicates that graphene was n-doped by ZZO without additional chemical doping process and ZZO can perform an additional role as an ETL of iOSCs. The iOSCs with ZZO and the n-doped CVD-grown graphene cathodes achieved the identical PCE (≈7.5%), slightly higher J_{SC}, but slightly lower FF than iOSCs with ITO cathodes; the higher J_{SC} was mainly attributed to higher transmittance of graphene, higher optical electric field of the photo-active layer on graphene/ZZO, and consequent increase in light harvesting of photo-active layer on graphene cathode than ITO. Meanwhile, the lowering of FF seemed to be due mainly to higher R_s and charge trapping caused by presence of impurities such as PMMA residues on the graphene surface. To understand the J–V characteristics, we compared G_{max} values of each device and exploited the light-intensity dependency of V_{OC} and J_{SC} to analyze recombination kinetics; results suggested that higher G_{max} of graphene device than ITO device makes higher J_{SC} and nongeminate recombination in the device with graphene cathode reduced FF. We believe the fact that the device with graphene electrodes achieved the same PCE as the device with ITO suggests that graphene is applicable as a transparent conducting electrode to replace ITO.

Experimental Section

Graphene Electrodes Preparation: Graphene was synthesized on Cu foil (Alpha Aesar) by chemical vapor deposition (CVD) method in a quartz tube. The Cu foil was loaded into a CVD chamber and heated to 1060 °C with H_2 gas inflow at 15 sccm after evacuation of the chamber (≈15 mTorr). After annealing for 30 min, CH_4 gas was additionally injected at 60 sccm for 30 min at the same temperature and the sample was rapidly cooled to room temperature while maintaining H_2 gas flow. Poly(methyl methacrylate) (PMMA) was spin coated as a supporting layer on the Cu foil, and an etchant (CE-100, Transene) was used to etch the Cu foil to transfer graphene onto the substrates. Then, acetone was used to remove the PMMA supporting layer. This transfer process was repeated three times to achieve three-layer stacked graphene for use as a cathode of iOSCs.

Preparation of the ZnO and Zonyl-Added ZnO Precursor: To make the ZnO precursor solution, 1 g of Zinc acetate dihydrate ($Zn(CH_3COO)_2{\cdot}2H_2O$, Sigma-Aldrich) and 0.28 g of ethanolamine as a stabilizer were dissolved in 10 mL of a solvent composed of 2-methoxyethanol ($CH_3OCH_2CH_2OH$, Sigma-Aldrich, 99.8%) and methanol (1:1 vol%) under vigorous stirring. Zonyl-added ZnO precursor was obtained by addition of 0.8 vol% Zonyl to ZnO precursor.

Solar Cell Device Fabrication: Devices were fabricated on graphene transferred on glass with $R_s \approx 300\ \Omega\ sq^{-1}$ or ITO-coated glass with $R_s \approx 15\ \Omega\ sq^{-1}$. Graphene was used after rinsing with acetone and iso-propanol without sonication; ITO was used after sonication with acetone and iso-propanol. To prevent graphene from peeling off during measurement, a 100-nm-thick Al layer was thermally evaporated at the edge of the graphene. Zonyl-added ZnO precursor solution was spin-coated at 1000 rpm for 60 s on graphene or ITO. UV-ozone treatment was not used, because it can damage graphene. After spin coating, the samples were annealed at 150 °C for 1 h. As a photo-active layer, a blend of 10 mg of PTB7 and 15 mg of $PC_{71}BM$ were dissolved in 1 mL of a mixed solvent chlorobenzene:1,8-diiodoctane (97:3 vol%). The solution was filtered through a 0.45 μm-pore PTFE syringe filter, then the blend was spin coated at 1000 rpm for 30 s and then annealed at 70 °C for 10 min. The samples were loaded into a high-vacuum chamber (2×10^{-7} Torr), and then MoO_3 and Ag (5 nm and 100 nm) were thermally evaporated as a hole extraction interfacial layer and an anode layer in sequence. Metallic shadow masks were used to define the photo-active area where bottom cathodes and Ag anodes overlapped; the pixel areas were 0.04 cm^2. The complete devices were encapsulated by a glass lid using UV-curable resin.

Graphene Field-Effect Transistors (GFETs) Fabrication: Au 60 nm/Ti 3 nm for source-drain electrodes were thermally evaporated through shadow masks onto a monolayer graphene sheet which was on a 300 nm-thick SiO_2/Si substrate. For doping of Zonyl-added ZnO on graphene, Zonyl-added ZnO film was formed on the graphene surface under the same conditions applied to solar cell fabrication.

Characterization and Measurement: The J–V characteristics of solar cell devices were measured using a Keithley 2400 source measurement unit under a simulated illumination generated by a Newport 69907 solar simulator. The illumination intensity was determined based on a single-crystal silicon reference cell (SRC-1000-TC-QZ-N, VLSI standards incorporated, Oriel Newport). EQEs of devices were measured using the EQE measurement system of PV Measurements (Model QEX7) in ambient condition. Electrical transport properties of GFETs were measured using a probe station in an N_2-filled glove box.

UV–vis absorption and transmittance were measured using a UV–visible spectrometer (S-3100, SCINCO). Raman spectra were collected using a confocal Raman microscope (Alpha 300R, Witec).

Supporting Information

Supporting Information is available from the Wiley Online Library or from the author.

Acknowledgements

This work was supported by the Center for Advanced Soft-Electronics funded by the Ministry of Science, ICT and Future Planning as Global Frontier Project (CASE-2014M3A6A5060947). This work was also supported by the National Research Foundation of Korea (NRF) grant funded by the Korea government (MSIP) (NRF-2013R1A2A2A01068753). Work at Los Alamos was supported by Center for Integrated Nanotechnologies, a U.S. DOE BES user facility, and LANL LDRD Program.

Received: January 26, 2016
Revised: March 26, 2016
Published online: April 25, 2016

[1] a) S. Bae, H. Kim, Y. Lee, X. Xu, J.-S. Park, Y. Zheng, J. Balakrishnan, T. Lei, H. R. Kim, Y. I. Song, Y.-J. Kim, K. S. Kim, B. Ozyilmaz, J.-H. Ahn, B. H. Hong, S. Iijima, *Nat. Nanotechnol.* **2010**, *5*, 574; b) J. Wu, H. A. Becerril, Z. Bao, Z. Liu, Y. Chen, P. Peumans, *Appl. Phys. Lett.* **2008**, *92*, 263302; c) J. O. Hwang, J. S. Park, D. S. Choi, J. Y. Kim, S. H. Lee, K. E. Lee, Y.-H. Kim, M. H. Song, S. Yoo, S. O. Kim, *ACS Nano* **2012**, *6*, 159; d) S. H. Lee, H. W. Kim, J. O. Hwang, W. J. Lee, J. Kwon, C. W. Bielawski, R. S. Ruoff, S. O. Kim, *Angew. Chem. Int. Ed.* **2010**, *49*, 10084; e) D. H. Wang, J. K. Kim, J. H. Seo, I. Park, B. H. Hong, J. H. Park, A. J. Heeger, *Angew. Chem. Int. Ed.* **2013**, *52*, 2874; f) H.-K. Seo, T.-S. Kim, C. Park, W. Xu, K. Baek, S.-H. Bae, J.-H. Ahn, K. KimH. C. Choi, T.-W. Lee, *Sci. Rep.* **2015**, *5*, 16710.

[2] a) K. S. Novoselov, A. K. Geim, S. V. Morozov, D. Jiang, Y. Zhang, S. V. Dubonos, I. V. Grigorieva, A. A. Firsov, *Science* **2004**, *306*, 666; b) R. R. Nair, P. Blake, A. N. Grigorenko, K. S. Novoselov, T. J. Booth, T. Stauber, N. M. R. Peres, A. K. Geim, *Science* **2008**, *320*, 1308; c) C. Lee, X. Wei, J. W. Kysar, J. Hone, *Science* **2008**, *321*, 385; d) W. Xu, H.-K. Seo, S.-Y. Min, H. Cho, T.-S. Lim, C.-Y. Oh, Y. Lee, T.-W. Lee, *Adv. Mater.* **2014**, *26*, 3459.

[3] a) D.-Y. Wang, I.-S. Huang, P.-H. Ho, S.-S. Li, Y.-C. Yeh, D.-W. Wang, W.-L. Chen, Y.-Y. Lee, Y.-M. Chang, C.-C. Chen, C.-T. Liang, C.-W. Chen, *Adv. Mater.* **2013**, *25*, 4521; b) Y. Wang, X. Chen, Y. Zhong, F. Zhu, K. P. Loh, *Appl. Phys. Lett.* **2009**, *95*, 063302; c) Y. Wang, S. W. Tong, X. F. Xu, B. Özyilmaz, K. P. Loh, *Adv. Mater.* **2011**, *23*, 1514; d) H. Park, J. Kong, *Adv. Energy Mater.* **2014**, *4*, 1301280; e) B. H. Lee, J.-H. Lee, Y. H. Kahng, N. Kim, Y. J. Kim, J. Lee, T. Lee, K. Lee, *Adv. Funct. Mater.* **2014**, *24*, 1847; f) H. Park, S. Chang, X. Zhou, J. Kong, T. Palacios, S. Grade ak, *Nano Lett.* **2014**, *14*, 5148; g) K.-S. Shin, H. Jo, H.-J. Shin, W. M. Choi, J.-Y. Choi, S.-W. Kim, *J. Mater. Chem.* **2012**, *22*, 13032; h) H. Park, S. Chang, M. Smith, S. Gradecak, J. Kong, *Sci. Rep.* **2013**, *3*, 1581; i) H. Kim, S.-H. Bae, T.-H. Han, K.-G. Lim, J.-H. Ahn, T.-W. Lee, *Nanotechnology* **2014**, *25*, 014012; j) A. R. bin Mohd Yusoff, D. Kim, F. K. Schneider, W. J. da Silva, J. Jang, *Energy Environ. Sci.* **2015**, *8*, 1523; k) K. Kim, S.-H. Bae, C. T. Toh, H. Kim, J. H. Cho, D. Whang, T.-W. Lee, B. Özyilmaz, J.-H. Ahn, *ACS Appl. Mater. Interfaces* **2014**, *6*, 3299; l) T.-H. Han, Y. Lee, M.-R. Choi, S.-H. Woo, S.-H. Bae, B. H. Hong, J.-H. Ahn, T.-W. Lee, *Nat. Photonics* **2012**, *6*, 105; m) H. Cho, S. D. Kim, T.-H. Han, I. Song, J.-W. Byun, Y.-H. Kim, S. Kwon, S.-H. Bae, H. C. Choi, J.-H. Ahn, T.-W. Lee, *2D Mater.* **2015**, *2*, 014002; n) S.-H. Bae, O. Kahya, B. K. Sharma, J. Kwon, H. J. Cho, B. Özyilmaz, J.-H. Ahn, *ACS Nano* **2013**, *7*, 3130; o) Y.-Y. Lee, K.-H. Tu, C.-C. Yu, S.-S. Li, J.-Y. Hwang, C.-C. Lin, K.-H. Chen, L.-C. Chen, H.-L. Chen, C.-W. Chen, *ACS Nano* **2011**, *5*, 6564; p) T.-H. Han, S.-J. Kwon, H.-K. Seo, T.-W. Lee, *2D Mater.* **2016**, *3*, 014003; q) T.-H. Han, S.-J. Kwon, N. Li, H.-K. Seo, W. Xu, K. S. Kim, T.-W. Lee, *Angew. Chem. Int. Ed.* **2016**, *55*, DOI: 10.1002/anie.201600414; r) S.-J. Byun, H. Lim, G.-Y. Shin, T.-H. Han, S. H. Oh, J.-H. Ahn, H. C. Choi, T.-W. Lee, *J. Phys. Chem. Lett.* **2011**, *2*, 493.

[4] J. You, L. Dou, K. Yoshimura, T. Kato, K. Ohya, T. Moriarty, K. Emery, C.-C. Chen, J. Gao, G. Li, Y. Yang, *Nat. Commun.* **2013**, *4*, 1446.

[5] Y. Liu, J. Zhao, Z. Li, C. Mu, W. Ma, H. Hu, K. Jiang, H. Lin, H. Ade, H. Yan, *Nat. Commun.* **2014**, *5*, 5293.

[6] A. K. K. Kyaw, X. W. Sun, C. Y. Jiang, G. Q. Lo, D. W. Zhao, D. L. Kwong, *Appl. Phys. Lett.* **2008**, *93*, 221107.

[7] L.-M. Chen, Z. Hong, G. Li, Y. Yang, *Adv. Mater.* **2009**, *21*, 1434.

[8] Y. Sun, J. H. Seo, C. J. Takacs, J. Seifter, A. J. Heeger, *Adv. Mater.* **2011**, *23*, 1679.

[9] H. Choi, J. S. Park, E. Jeong, G.-H. Kim, B. R. Lee, S. O. Kim, M. H. Song, H. Y. Woo, J. Y. Kim, *Adv. Mater.* **2011**, *23*, 2759.

[10] M. Ahmadi, K. Mirabbaszadeh, S. Salari, H. Fatehy, *Electron. Mater. Lett.* **2014**, *10*, 951.

[11] D. Wei, Y. Liu, Y. Wang, H. Zhang, L. Huang, G. Yu, *Nano Lett.* **2009**, *9*, 1752.

[12] Z. Jin, J. Yao, C. Kittrell, J. M. Tour, *ACS Nano* **2011**, *5*, 4112.

[13] C. Zhang, L. Fu, N. Liu, M. Liu, Y. Wang, Z. Liu, *Adv. Mater.* **2011**, *23*, 1020.

[14] B. Guo, Q. Liu, E. Chen, H. Zhu, L. Fang, J. R. Gong, *Nano Lett.* **2010**, *10*, 4975.

[15] W. Xu, L. Wang, Y. Liu, S. Thomas, H.-K. Seo, K.-I. Kim, K. S. Kim, T.-W. Lee, *Adv. Mater.* **2015**, *27*, 1619.

[16] W. Xu, T.-S. Lim, H.-K. Seo, S.-Y. Min, H. Cho, M.-H. Park, Y.-H. Kim, T.-W. Lee, *Small* **2014**, *10*, 1999.

[17] K. C. Kwon, K. S. Choi, S. Y. Kim, *Adv. Funct. Mater.* **2012**, *22*, 4724.

[18] M. Si, W. J. Choi, Y. J. Jeong, Y. K. Lee, J.-J. Kim, J.-O. Lee, *Phys. E* **2016**, *80*, 115.

[19] J. Meyer, P. R. Kidambi, B. C. Bayer, C. Weijtens, A. Kuhn, A. Centeno, A. Pesquera, A. Zurutuza, J. Robertson, S. Hofmann, *Sci. Rep.* **2014**, *4*, 5380.

[20] S. Sanders, A. Cabrero-Vilatela, P. R. Kidambi, J. A. Alexander-Webber, C. Weijtens, P. Braeuninger-Weimer, A. I. Aria, M. M. Qasim, T. D. Wilkinson, J. Robertson, S. Hofmann, J. Meyer, *Nanoscale* **2015**, *7*, 13135.

[21] S. Tongay, M. Lemaitre, X. Miao, B. Gila, B. R. Appleton, A. F. Hebard, *Phys. Rev. X* **2012**, *2*, 11002.

[22] G. Kresse, J. Furthmüller, *Phys. Rev. B* **1996**, *54*, 11169.

[23] G. Kresse, J. Hafner, *Phys. Rev. B* **1993**, *47*, 558.

[24] G. Kresse, J. Furthmüller, *Comput. Mater. Sci.* **1996**, *6*, 15.

[25] J. P. Perdew, K. Burke, M. Ernzerhof, *Phys. Rev. Lett.* **1996**, *77*, 3865.

[26] D. Vanderbilt, *Phys. Rev. B* **1990**, *41*, 7892.

[27] G. Kresse, J. Hafner, *J. Phys. Condens. Matter* **1994**, *6*, 8245.

[28] J. Klimeš, D. R. Bowler, A. Michaelides, *Phys. Rev. B* **2011**, *83*, 195131.

[29] M. Shishkin, G. Kresse, *Phys. Rev. B* **2007**, *75*, 235102.

[30] M. Shishkin, M. Marsman, G. Kresse, *Phys. Rev. Lett.* **2007**, *99*, 246403.

[31] M. Vosgueritchian, D. J. Lipomi, Z. Bao, *Adv. Funct. Mater.* **2012**, *22*, 421.

[32] N. M. Kovalchuk, A. Trybala, V. Starov, O. Matar, N. Ivanova, *Adv. Colloid Interface Sci.* **2014**, *210*, 65.

[33] Y. Kim, J. M. Yoo, H. R. Jeon, B. H. Hong, *Phys. Chem. Chem. Phys.* **2013**, *15*, 18353.

[34] Y. Kim, J. Park, J. Kang, J. M. Yoo, K. Choi, E. S. Kim, J.-B. Choi, C. Hwang, K. S. Novoselov, B. H. Hong, *Nanoscale* **2014**, *6*, 9545.

[35] Y. Kim, J. Ryu, M. Park, E. S. Kim, J. M. Yoo, J. Park, J. H. Kang, B. H. Hong, *ACS Nano* **2014**, *8*, 868.

[36] A. Das, S. Pisana, B. Chakraborty, S. Piscanec, S. K. Saha, U. V. Waghmare, K. S. Novoselov, H. R. Krishnamurthy, A. K. Geim, A. C. Ferrari, A. K. Sood, *Nat. Nanotechnol.* **2008**, *3*, 210.

[37] S. Pisana, M. Lazzeri, C. Casiraghi, K. S. Novoselov, A. K. Geim, A. C. Ferrari, F. Mauri, *Nat. Mater.* **2007**, *6*, 198.

[38] H.-J. Shin, W. M. Choi, D. Choi, G. H. Han, S.-M. Yoon, H.-K. Park, S.-W. Kim, Y. W. Jin, S. Y. Lee, J. M. Kim, J.-Y. Choi, Y. H. Lee, *J. Am. Chem. Soc.* **2010**, *132*, 15603.

[39] J. Bardeen, *Phys. Rev.* **1947**, *71*, 717.

[40] L. J. Brillson, Y. Lu, *J. Appl. Phys.* **2011**, *109*, 121301.

[41] M. W. Allen, S. M. Durbin, *Appl. Phys. Lett.* **2008**, *92*, 122110.

[42] Z. He, C. Zhong, X. Huang, W.-Y. Wong, H. Wu, L. Chen, S. Su, Y. Cao, *Adv. Mater.* **2011**, *23*, 4636.

[43] Q. Zhang, B. Kan, F. Liu, G. Long, X. Wan, X. Chen, Y. Zuo, W. Ni, H. Zhang, M. Li, Z. Hu, F. Huang, Y. Cao, Z. Liang, M. Zhang, T. P. Russell, Y. Chen, *Nat. Photonics* **2015**, *9*, 35.

[44] S. R. Cowan, A. Roy, A. J. Heeger, *Phys. Rev. B* **2010**, *82*, 245207.

[45] C. Liu, X. Hu, C. Zhong, M. Huang, K. Wang, Z. Zhang, X. Gong, Y. Cao, A. J. Heeger, *Nanoscale* **2014**, *6*, 14297.

[46] A. Foertig, J. Kniepert, M. Gluecker, T. Brenner, V. Dyakonov, D. Neher, C. Deibel, *Adv. Funct. Mater.* **2014**, *24*, 1306.

[47] P. Schilinsky, C. Waldauf, C. J. Brabec, *Appl. Phys. Lett.* **2002**, *81*, 3885.

[48] I. Riedel, J. Parisi, V. Dyakonov, L. Lutsen, D. Vanderzande, J. C. Hummelen, *Adv. Funct. Mater.* **2004**, *14*, 38.

[49] D. I. Son, T. W. Kim, J. H. Shim, J. H. Jung, D. U. Lee, J. M. Lee, W. I. Park, W. K. Choi, *Nano Lett.* **2010**, *10*, 2441.